

A bionic robotic fish with a dielectric elastomer

Chenghong Zhang(张成红)

Citation: Chin. Phys. B, 2025, 34 (**4**): 048702. DOI: 10.1088/1674-1056/adacc9
Journal homepage: http://cpb.iphy.ac.cn; http://iopscience.iop.org/cpb

What follows is a list of articles you may be interested in

Disorder-to-order transition induced by spontaneous cooling regulation in robotic active matter

Shuaixu Hou(侯帅旭), Gao Wang(王高), Xingyu Ma(马星宇), Chuyun Wang(汪楚云), Peng Wang(王鹏), Huaicheng Chen(陈怀城), Liyu Liu(刘雳宇), and Jing Wang(王璟)
Chin. Phys. B, 2024, 33 (**7**): 078701. DOI: 10.1088/1674-1056/ad4327

Bio-inspired environmental adaptability of swarm active matter

Yangkai Jin(金阳凯), Gao Wang(王高), Daming Yuan(袁大明), Peilong Wang(王培龙), Jing Wang(王璟), Huaicheng Chen(陈怀城), Liyu Liu(刘雳宇), and Xingjie Zan(昝兴杰)
Chin. Phys. B, 2023, 32 (**8**): 088703. DOI: 10.1088/1674-1056/acd688

Orderly hysteresis in field-driven robot swarm active matter

Yanping Liu(刘艳萍), Gao Wang(王高), Peilong Wang(王培龙), Daming Yuan(袁大明), Shuaixu Hou(侯帅旭), Yangkai Jin(金阳凯), Jing Wang(王璟), and Liyu Liu(刘雳宇)
Chin. Phys. B, 2023, 32 (**6**): 068701. DOI: 10.1088/1674-1056/acc803

Unidirectional rotation of circles driven by chiral active particles

Jiamin Chen(陈佳敏), Xiaolin Zhou(周晓琳), Linxi Zhang(章林溪)
Chin. Phys. B, 2018, 27 (**11**): 118701. DOI: 10.1088/1674-1056/27/11/118701

A bionic robotic fish with a dielectric elastomer

Chenghong Zhang(张成红)[1,2,†]

[1] *Key Laboratory of Advanced Manufacturing Technology, Ministry of Education, Guizhou University, Guiyang* 550025, *China*
[2] *School of Electronics & Information Engineering, Guiyang University, Guiyang* 550005, *China*

(Received 7 October 2024; revised manuscript received 28 December 2024; accepted manuscript online 22 January 2025)

Dielectric elastomer actuators (DEAs) are promising enabling devices which can be used in a wide range of robots, artificial muscles, and microfluidics. They are characterized by high actuating strain, low cost and noise, and high energy density and efficiency. There are three main challenges for enabling DEs to become actuators: (i) developing suitable and compatible electrode materials; (ii) effectively isolating the actuator electrode from the surrounding fluid; and (iii) creating a rigid frame that usually requires prestraining of the dielectric layer. The use of robotic fish in water is an important application field of biomimetic soft robots. At present, most underwater robotic fish use spiral propulsion, which has several problems, including propulsion efficiency, position controllability and aquatic organism involvement. To provide solutions, the research and development of underwater robotic fish that imitate the fins and body propulsion of fish and the use of soft underwater robotic fish are in full adoption. This project involves the research and development of a bionic soft underwater robot fish with a software driver, which can imitate swimming via the tail fin and body of a fish, especially with respect to stable swimming propulsion, to successfully develop high-performance soft underwater robot fish. In addition, to imitate the unstable swimming movements of fish, such as turning and sharp acceleration and deceleration, robot fish that use DE drivers with good flexibility and high strain have been researched and developed.

Keywords: dielectric elastomer actuator (DEA), soft robot fish, motion analysis

PACS: 87.85.St, 45.40.Ln, 47.11.–j, 47.10.–g

DOI: 10.1088/1674-1056/adacc9 **CSTR:** 32038.14.CPB.adacc9

1. Introduction

A dielectric elastomer (DE) is an electroactive polymer that is capable of converting electrical energy into mechanical energy, which enables a drive function.[1] The drive mechanism of DE systems was first discovered by Wilhelmm in the 19th century.[2] In 1880, the driving principle of a DE was tested for the first time.[3] When the input driving voltage increased, the surface area of the DE film increased, and the thickness decreased.

Owing to its unique advantages of a low elastic modulus, large deformation range, high energy density and fast response speed, a dielectric elastomer actuator (DEA) also has these excellent properties and is widely used in driving a variety of DE soft robots. The dielectric layer is usually a silicon-based or acrylic-based polymer (e.g., polydimethylsiloxane or 3M's very high-bond acrylic adhesive). Electrodes are generally composed of deposited metals, carbon particles or nanotubes, ionic gels, or ionized hydrogels.[4] DEAs show great potential in the fields of microrobotics, biomimetic robots, artificial muscles, and microfluidics.[5–9] Recently, MIT successfully designed a microflexible flapping wing robot that is resistant to damage flight via a self-healing dielectric elastomer drive unit.[10] The DEA process is an energy conversion process coupled with multiple physical fields. It is also affected by the material's own properties, such as the dielectric constant, elastic modulus and viscoelasticity, as well as external factors, such as the material's frequency, temperature, and prestretch ratio, resulting in very complex nonlinear characteristics for the DEA system.[11]

Tang has also developed a flexible bionic pipe robot driven by DEs, which is capable of crawling in a subcentimeter pipe.[12] In its most basic form, a DEA is composed of an elastic medium sandwiched between a pair of flexible electrodes. Liu developed a soft triboelectric robot with a maximum crawling speed of 14.9 mm/s.[13] In 2016, the first swimming robot using piezoelectric elastomers was proposed, which mimics the movement of jellyfish.[14] Inspired by fish with swinging body/tail fins, Jiao *et al*. developed a DE bionic robotic fish.[15] Shintake *et al*. created a jellyfish robot with a single piezoelectric film structure and a robotic fish with a double piezoelectric film structure.[16] By using dielectric elastomer minimum energy structures (DEMES), Tang *et al*. developed a frog-shaped robot.[17] Inspired by breaststroke movements, Wang *et al*. made breaststroke robotic fish by imitating frog legs with two DEA.[18] Xu *et al*. developed a DEA with a solid–liquid interpenetrating network structure and used it to make a soft bionic ray robot.[19] Zhang *et al*. used hydrogel as the body and DEA as the driving unit to produce manta ray like soft robot fish.[20]

Research is underway on biomimetic robotic fish using soft actuators that simulate swimming using fish tail fins and

[†]Corresponding author. E-mail: zhangchenghongcn@aliyun.com

© 2025 Chinese Physical Society and IOP Publishing Ltd. All rights, including for text and data mining, AI training, and similar technologies, are reserved.

the back of the body.[21] Especially in terms of stable swimming propulsion, high-performance soft water robots have been successfully developed. In order to simulate the unstable swimming movements of a fish, such as turning and accelerating and decelerating, a robotic fish using a DEA with good flexibility and high strain was studied.

The robotic fish actuators are based on DEMES. In order to imitate the bending motion of the left and right sides of a fish, a drive unit connecting two bending actuators was made. In order to identify the response characteristics of the driving unit, the relationship between the driving voltage of the input signal and the motion output of the bending actuator is studied. A robot fish was designed, and the swimming speed at each frequency was obtained by changing the frequency for swimming experiments.

2. The use of demes

When a DE is used as a driver, it needs to be prestretched. The actuators are prepared using DE minimum energy structures (DEMESs). The elastic body takes the surface with the smallest area under any boundary conditions and thus constructs the minimum energy structure. By adjusting the rigidity of the plastic frame, unidirectional bending can be produced. DEMESs are made by attaching a prestretched DE film to a flexible, nonstretchable frame and changing its bending state by controlling the voltage. When relaxed, the structure bends until the tension on the prestretched film and the bending moment of the frame are in balance, resulting in a grip-like shape.

2.1. Design of the bending actuator

The curved drive made according to the parameters of Table 1 is shown in Fig. 2. Figure 1 shows the structure of the bent drive, where l is the width, w is the height, t is the thickness of the substrate, p is the thickness of the fixed material, q is the width of the fixed material, s is the distance between fixed materials, and r is the radius of the semicircle.

Table 1. Parameters of the bending drive.

Basement material	Material of fixed material	Prestretch	w (mm)	p (mm)	q (mm)	t (mm)	l (mm)	s (mm)	r (mm)
PET	PET	extension ratio four	57	2	30	0.125	88	8	15

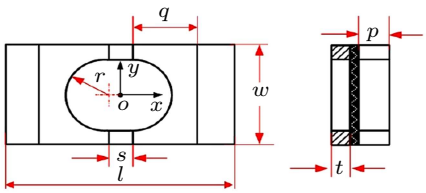


Fig. 1. Structure of a bent drive.

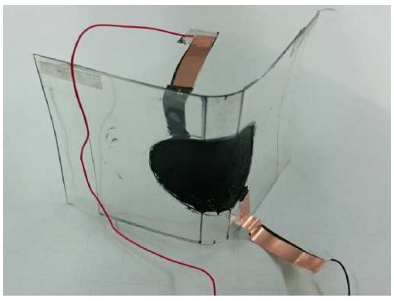


Fig. 2. Curved drive.

2.2. Response characteristics

To confirm the response characteristics of the DE driver, the relationship between the driving voltage of the input signal and the output of the driver is studied. Figure 3 shows a schematic diagram of measuring the angle of a DEA.

Curve fitting is a method used in mathematics and statistics to describe the tendency of the distribution of a set of data points. A common method for curve fitting is to use least squares to find the best fitting parameters by minimizing the sum of squares of residuals. The polynomial equation for fitting the function n is as follows:

$$y = a_0 + a_1 x + a_2 x^2 + \cdots + a_n x^n, \tag{1}$$

where y represents the dependent variable, x represents the independent variable, $a_0, a_1, \ldots, a_n$ represent the fitting parameter, and n is the order of the polynomial.

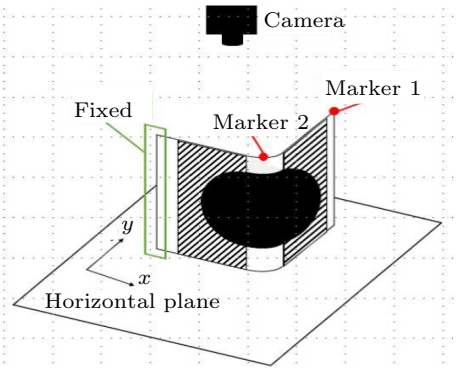


Fig. 3. Schematic diagram of measuring the angle of a DEA.

Figure 4 shows the output when a 4-kV stepping signal is input, approximating a primary delay system. The increase continues until after approximately 18 s, after which it remains unchanged, and the measurement ends after approximately 22 s. The maximum change in angle occurred 18 s after the end of the measurement, with an average angle of

42.2°. The time to reach the maximum displacement of 63.2% can be understood as the base time constant $\tau = 0.3$ s for the exponential growing region. In addition, if the response time is set as the time to reach 95% of the maximum displacement, it is 11.6 seconds. Compared with flat plate drives, the response time is shorter. This is due to the flat motion not being converted into a curved area.

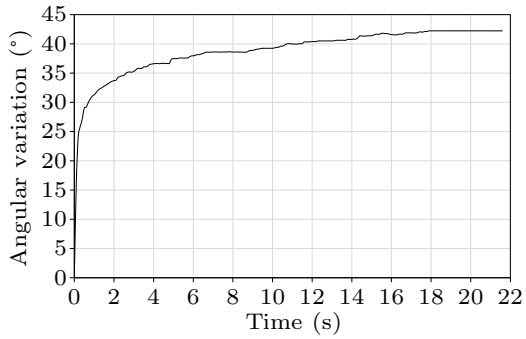


Fig. 4. Step response of the DEA.

When the input with a sine wave varies from 0 to 4 kV, figure 5 shows the gain curve of the output amplitude at a frequency of 0.1 Hz, and figure 6 shows the corresponding phase curve of the input signal. The input voltage frequencies are 0.1 Hz, 0.5 Hz, 1 Hz, 3 Hz, 5 Hz, 6 Hz, 7 Hz, 9 Hz, and 10 Hz.

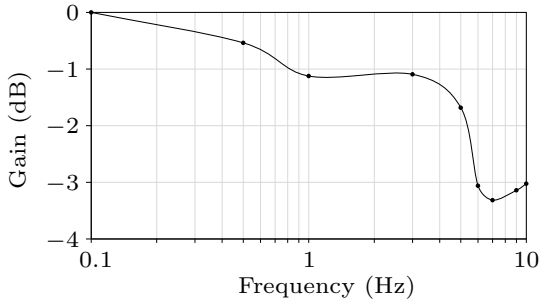


Fig. 5. Gain characteristics of the DEA.

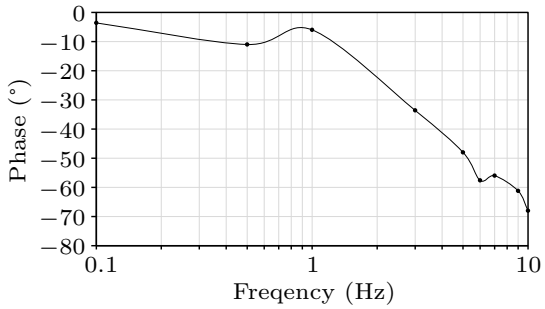


Fig. 6. Phase characteristics of the DEA.

The cutoff frequency with a gain of −3 dB is approximately 5.9 Hz, the highest drive frequency for the driver in this system. The phase deviation at this point is approximately −58°. Since the stability limit is −180°, the system is stable at 5.9 Hz.

Compared with that of a flat drive, the response frequency is improved. The reason may be affected by the difference between the action of the drive at 0.1 Hz and 0.5 Hz and the action after 3 Hz. Figures 7 and 8 show the motion trajectories at 0.1 Hz and 3 Hz. The origin is the fixed point in Fig. 3. Comparing the two, we can see that at 0.1 Hz, there is almost no movement in the center position; only the unfixed end is working, whereas at 3 Hz, the center mark position is also moving, at which time the entire drive is in motion. Since this operation suppresses the angle change after 3 Hz, the response frequency of the drive is improved.

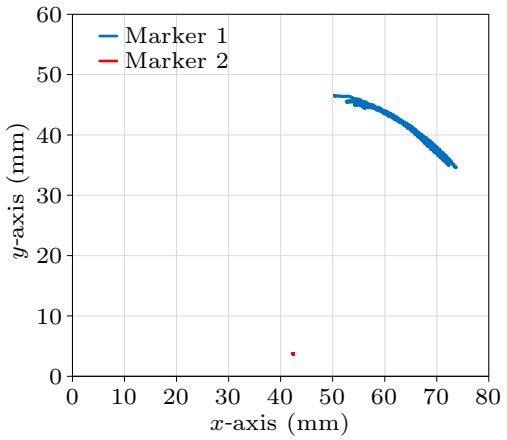


Fig. 7. Each marked motion trajectory at 0.1 Hz.

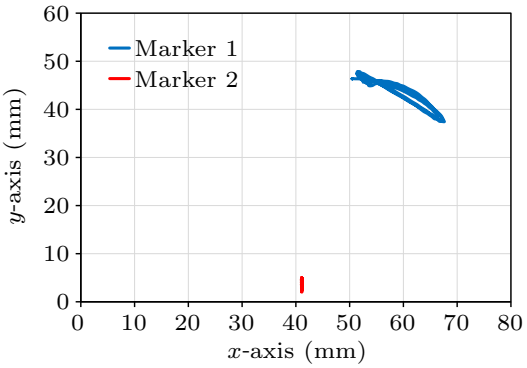


Fig. 8. Motion track of each mark at 3 Hz.

2.3. Advancement of serpentine motion

The principle by which a fish gains propulsion through its serpentine motion is shown in Fig. 9 and is the inertial force (the force pushing the fluid) due to the increase in amplitude.

The hydrodynamic characteristics of elongated organisms are the two-dimensional fluid force, which is determined by the shape of each section, and the inertial force, which is caused by the additional mass change instead of the length direction. This can be dealt with in terms of slender body theory, which constitutes the total fluid force of the section.

In the coordinate system of a slender body, as shown in Fig. 10, the lift direction l (x, t) when moving the slender body in the velocity v–x direction produces Δp changes in the y direction.

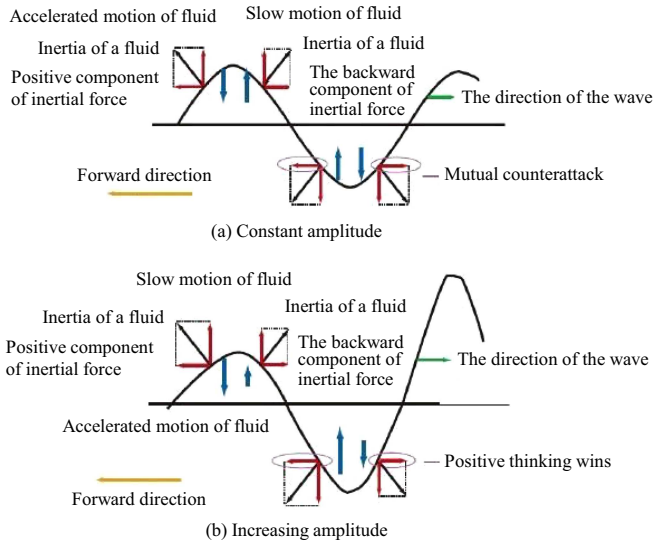


Fig. 9. Inertial force of fluctuating motion.

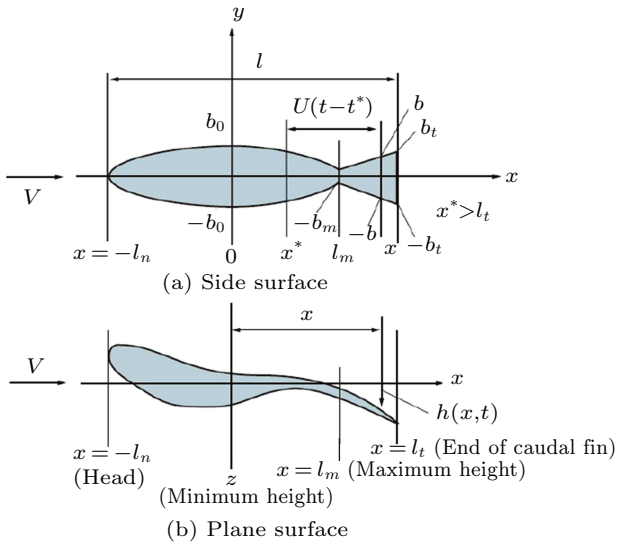


Fig. 10. Coordinate system of the slender body.

The propulsive force T_s based on the attraction acting on the edge is as follows.

$$T_s = \int_{-l_n}^{0} \left\{ \frac{1}{2} w^2 \frac{\partial A_{33}}{\partial x} \right\} \mathrm{d}x + \int_{l_m}^{l_t} \left\{ \frac{1}{2} (w - w^*)^2 \frac{\partial A_{33}}{\partial x} \right\} \mathrm{d}x. \quad (2)$$

Elongated creatures are characterized by changes in height to length. The added mass of the change thus contributes significantly to the propulsive force. If the body height at the tail is not reduced, then the propulsive force will be negative. Therefore, the thinner the tail is, the better. For a low aspect ratio swept-back wing with an almost triangular or near-triangular tail fin shape, it is most important that the terminal end is at the maximum width and swings here with the maximum amplitude.

3. DE actuator

3.1. Structure of the drive unit

To imitate the bending motion of the left and right sides of a fish, a driving unit connecting two bending drivers was created. To exploit the bending motion of the drive, the rotation center of the drive unit is as consistent as possible with the structure of the rotation center of the left and right bending drive structures. However, when the frequency of the bending drive is increased, the center of the drive will also move, so it is not a complete rotation motion, and the rotation center cannot be determined as one position. Therefore, a flexible structure is adopted, and the rotation center is not specified; however, the movement of the drive is utilized. According to the above conditions, the driving unit is as shown in Fig. 11. The driving unit adopts the structure of directly bonding one end of the two bending drives and connecting the other end through the connecting piece. The structure of the drive unit is shown in Fig. 12.

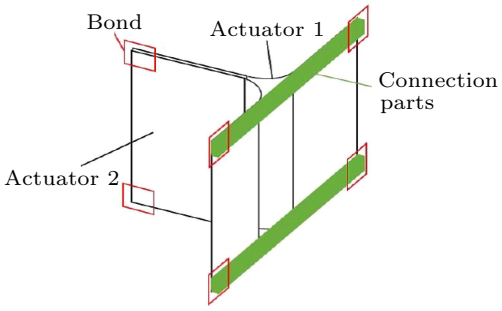


Fig. 11. Structure of the drive unit.

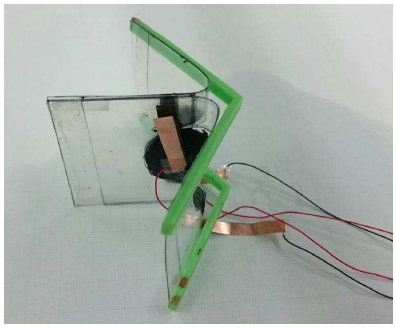


Fig. 12. Pilot drive.

This drive unit has the advantage of homogenizing the initial angle of the bent drive. The initial angle of the bent drive is difficult to fix each time because of the differences created when it is used. Since the structure is fixed by connecting parts so that the left and right angles are fixed, the initial conditions can be unified for all drives.

3.2. Drive experiments

3.2.1. Connection angle

Since the angle of the connection component is fixed, the setting is not affected by the initial state of the bent drive. To determine the angle of the connector, a drive test is carried out at every 30° angle to compare the drive performance.

Figure 13 shows the definition of the angle of the connector. The angle is divided into 5 cases: 30°, 60°, 90°, 120° and 150°.

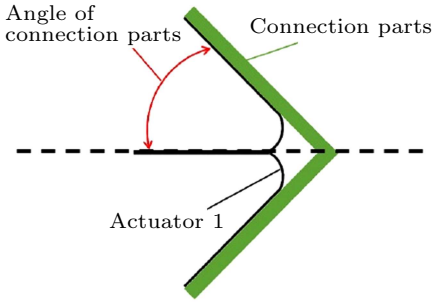


Fig. 13. Definition of the connector angle.

In the direction of the bending action in the horizontal direction, the ends of the drivers bonded to each other are fixed, and only 1 period of sinusoidal voltage with an amplitude of 0–4 kV and a frequency of 0.1 Hz is input to the driver on one side. The maximum value of the angle change of the connector and the maximum value of the force generated at the front end of the connector are measured. A schematic diagram of the measurement driver from the horizontal direction is shown in Figs. 14 and 15.

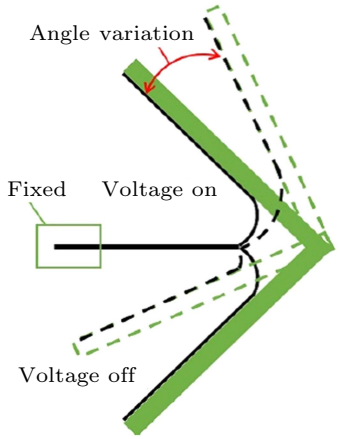


Fig. 14. Measurement of drive angle change.

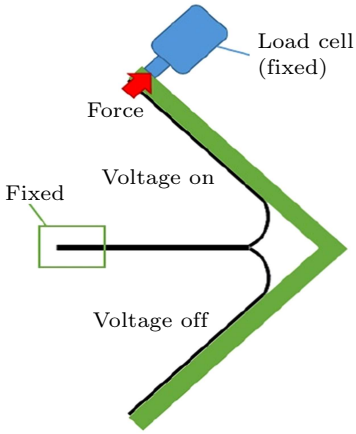


Fig. 15. Measurement of the driving force.

The angle change and the maximum value and product of the force of each angle of the connector are shown in Table 2.

The connector angle changes up to 90°. This may be because at angles of 30° and 60°, the elastomer in the electrode part becomes thicker because of greater bending and a decrease in the Maxwell stress. At angles of 120° and 150°, the area away from the deformation limit decreases.

To account for both the angle change and the force magnitude, the two values are compared after they are multiplied. The product value is maximized when the angle of the connector is 90°. When the angle of the connector is 60°, it is also larger than the product value of the other angles. Therefore, the two cases of 90° and 60° are studied.

Table 2. Measurement results of the angles of each connector.

Angle of connection	30°	60°	90°	120°	150°
Maximum angle change	7.9	14.5	17.5	16.7	8.7
Maximum generated force	11.08	11.46	10.31	7.26	2.29
Maximum angle change × maximum power	87.5	166.2	180.4	121.2	19.9

3.2.2. Input waveform

On the basis of the drive unit, the left and right drives need to be alternately driven. The previously used sine wave was able to drive smoothly, but even with a 180° phase deviation, the drivers on both sides were interfered with by the applied voltage. Therefore, when the driver on one side applies voltage, it is necessary to prevent the voltage from being applied completely to the other side. Thus, in the drive unit, rectangular voltage waves that differ by 180° are input. Figure 16 shows a 180° rectangular voltage difference in the input.

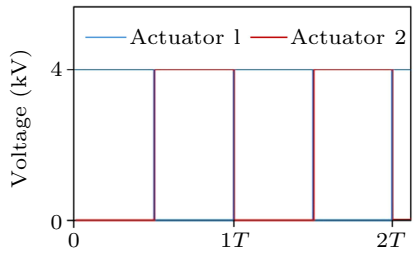


Fig. 16. Input rectangular voltage difference of 180°.

3.2.3. Measuring the angle change of the connector

The angle change is measured as a motion output via the following method. The measurements were made for two conditions where the angle of the connector was 60° and 90°.

The glued end between the drives is fixed in the direction where the bending action occurs in the horizontal direction, and the markers on the two points are configured at the center of the connector and the end of the connector. The x and y coordinates of the marks are measured for each period to find the change in slope of the two points. Figure 17 shows a schematic view of the measurement from the horizontal direction.

The measurement results indicate that when a rectangular wave of 0.1 Hz and 4 kV is input, when the angle of the connector is 60°, the angle change between the peaks is 18.7°;

when the angle of the connector is 90°, the angle change between the peaks is 21.1°. The angle between the sides is reduced by approximately 1/4 compared with the angle change of more than 40° for bending the driver cell. The reason is that when the drive on one side expands, the drive on the other side must be pushed to bend, thus hindering the action and limiting the action due to fixation.

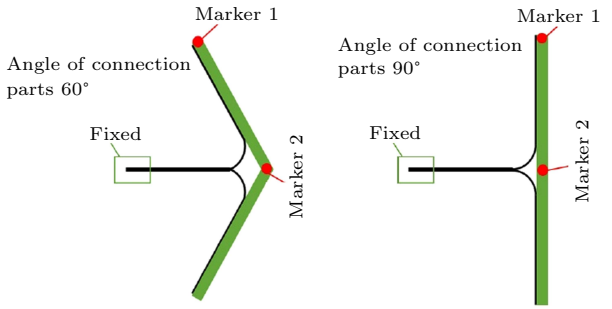


Fig. 17. Drive measurement mark position.

3.2.4. Response characteristics

To identify the response characteristics of the drive unit, the relationship between the drive voltage of the input signal and the motion output of the bending driver is studied.

The difference between the peaks on both sides of the driver when 1 cycle voltage is applied to drive the driver on both sides as the amplitude and the gain curve compared with the output amplitude at 0.1 Hz are shown in Fig. 18. Because the input is a rectangular wave, it is impossible to find the phase offset. Figures 19 and 20 show the angular motion output (angle change) at frequencies of 0.1 Hz, 0.5 Hz, 1 Hz, 3 Hz, 5 Hz, 6 Hz, 7 Hz, 9 Hz, and 10 Hz, for a total of 9 frequencies.

With a gain of −3 dB, the cutoff frequency for connecting devices at an angle of 60° is 6.1 Hz, and the cutoff frequency at 90° is 6.4 Hz. This can be considered the highest drive frequency of the drive unit in this system. At 60° and 90°, the gain is slowly reduced to 6 Hz and greatly reduced between 6 Hz and 7 Hz. The general characteristics are consistent compared with those of the curved driver cell; that is, the gain continues to be slowly reduced by half, and then the reduction is greater. The bending driver has a large reduction between 5 Hz and 6 Hz, and through unitization, the response frequency is increased by 0.2 Hz–0.5 Hz.

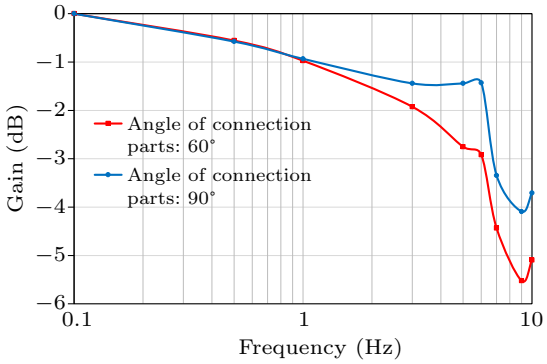


Fig. 18. Gain characteristics of the drive unit.

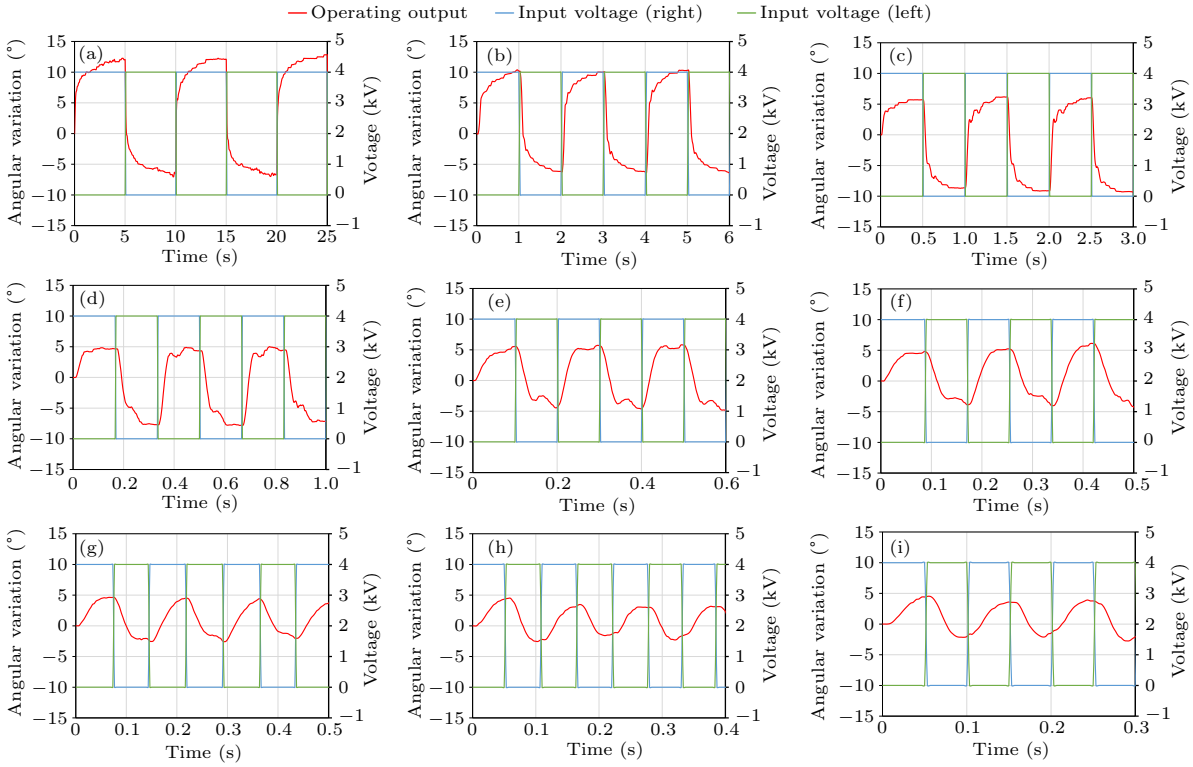


Fig. 19. Angular motion outputs when the connector angle is 60° and the frequencies are (a) 0.1 Hz, (b) 0.5 Hz, (c) 1 Hz, (d) 3 Hz, (e) 5 Hz, (f) 6 Hz, (g) 7 Hz, (h) 9 Hz, and (i) 10 Hz.

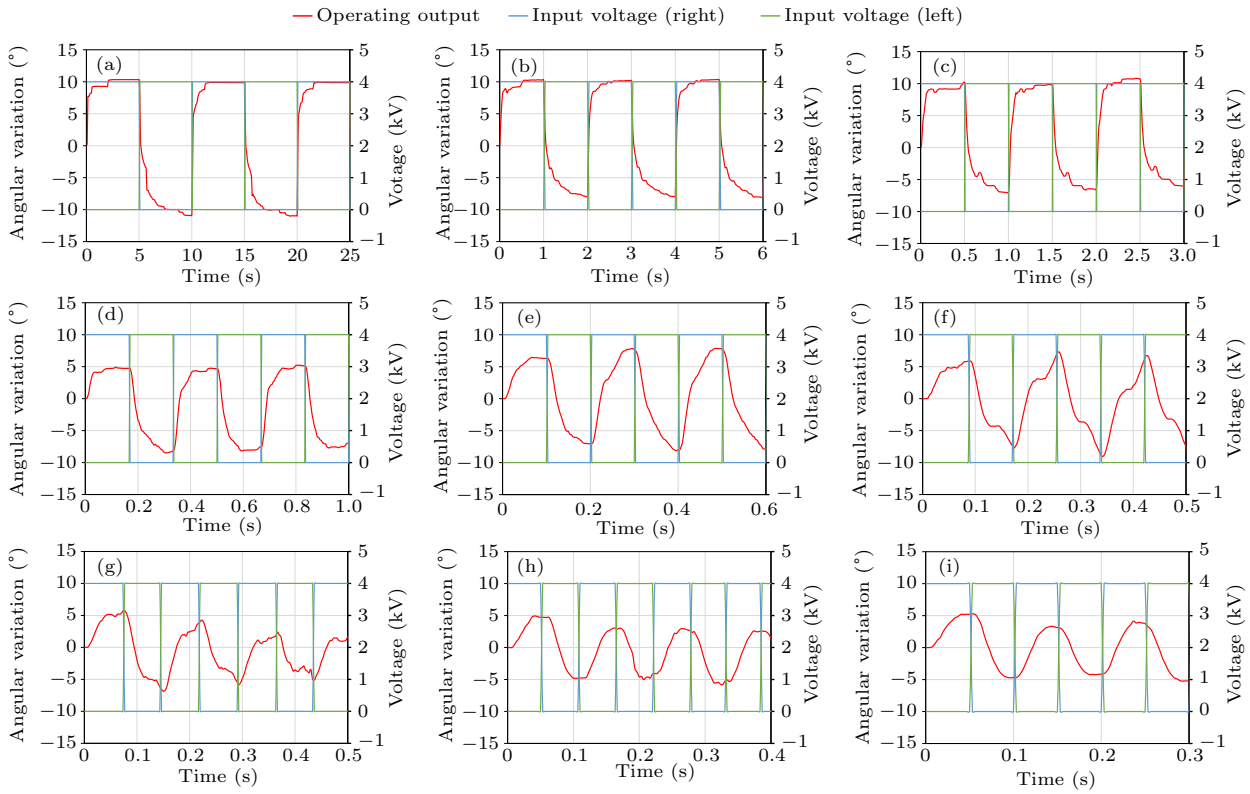


Fig. 20. Angular motion output when the connector angle is 90° and the frequencies are (a) 0.1 Hz, (b) 0.5 Hz, (c) 1 Hz, (d) 3 Hz, (e) 5 Hz, (f) 6 Hz, (g) 7 Hz, (h) 9 Hz, and (i) 10 Hz.

4. Robotic fish

4.1. Structure of robotic fish

One side of the connecting piece of the driving unit is the head, and the end directly bonded between the drives is installed with a tail fin made of CFRP. The rear end of the tail fin is the same as the drive fin, 57 mm, and the aspect ratio is approximately 2. The size of the caudal fin is shown in Fig. 21. In addition, the center and two front ends of the connector are weighted, and the buoyancy is adjusted by buoys.

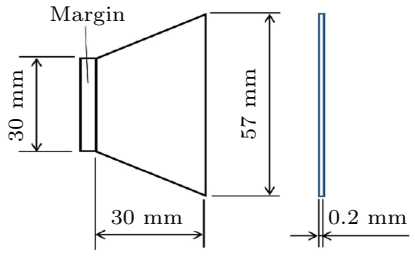


Fig. 21. Size of the tail fin.

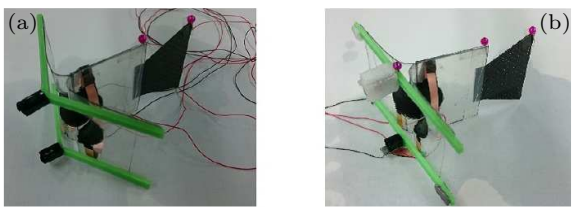


Fig. 22. Robot fish: (a) the connector angle is 60°, (b) the connector angle is 90°.

The actual trial production of the robotic fish is shown in Fig. 22. The specifications of the robot fish are shown in Table 3, and a schematic diagram of the robot fish is shown in Fig. 23.

Table 3. Models of robotic fish in water.

Body length (mm)	95
High (mm)	57
Weight (g)	12.6
Drive area (mm^2)	946.8

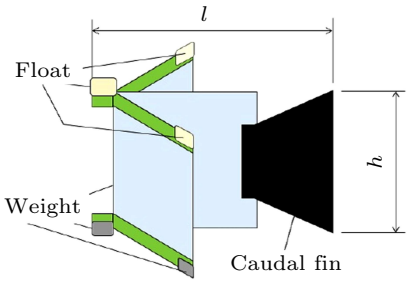


Fig. 23. Schematic diagram of the robotic fish.

4.2. Performance evaluation of robotic fish

4.2.1. Determination of swimming speed

The robot fish swims in an insulated fluid. By changing the frequency of the swimming experiment, the swimming speed at each frequency is obtained. The measurement method is to set a mark on the head, shoot the swimming process of the robot fish from the top with a high-speed camera at 300 fps,

obtain the middle 10-second video of swimming, and mark the distance along the straight direction (X-axis direction). The measurement is shown in Fig. 24.

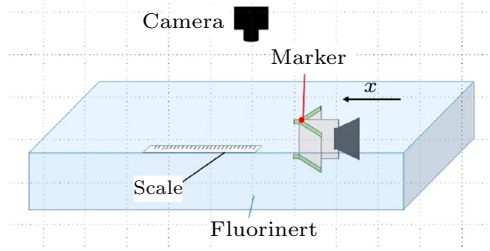


Fig. 24. Photograph of swimming speed.

Change occurs at a frequency of 1 Hz from 1 Hz to 10 Hz. Two kinds of robotic fish with connector angles of 60° and 90° are measured separately.

Figure 25 shows the swimming speed for each frequency. At 1 Hz, the swimming speed of the robot fish is relatively low, and the swimming speed of the robot fish with the connector angle of 60° is slightly higher than that of the robot fish with the connector angle of 90°. The swimming speed of a robot fish with a connector angle of 60° reaches a peak at 2 Hz and exceeded 14 mm/s, and then decreases rapidly. The robot fish swimming speed again reaches a higher speed at 9 Hz, exceeding 10 mm/s. The swimming speed of the robot fish with a connector angle of 90° reaches a peak at 2 Hz, but the speed is slightly higher than that of the robot swimming speed at a connector angle of 60°, which swims at a speed of more than 16 mm/s and then decreases rapidly. The robot fish swimming speed again reaches a higher speed at 9 Hz, more than 14 mm/s. As the frequency increases, the swimming speed of the robot fish fluctuates.

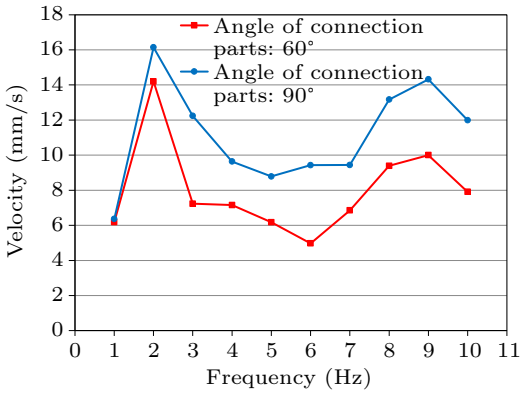


Fig. 25. Swimming speed at various frequencies.

In addition, at all frequencies, 90° connectors travel faster than 60° connectors do. The displacement ratio of the force has a greater effect on improving the swimming speed. The connector angle, whether 90° or 60°, reaches its highest speed at 2 Hz and peaks at 9 Hz. The robotic fish produces a primary modal resonance at 2 Hz and a secondary modal resonance at 9 Hz.

4.2.2. Promotion of work efficiency

To evaluate the propulsive work efficiency of the robot fish, the walk number S_w is calculated. The walk number is a dimensionless number that expresses the length of the body advancing under the tail fin over the distance and is also used for the propulsive efficiency of the actual fish. Most fish swim numbers are concentrated at approximately 0.6, expressed by formula (3) as the swimming speed U [in units of m/s], swimming frequency f (Hz), and body length L (m).

$$S_w = \frac{U}{f \cdot L}. \tag{3}$$

Figure 26 shows the number of walks S_w calculated according to formula (3). The robot fish can reach a maximum value of 0.085 at 2 Hz; after 3 Hz, the number of swarms decreases significantly. This value is approximately 1/7 that of fish.

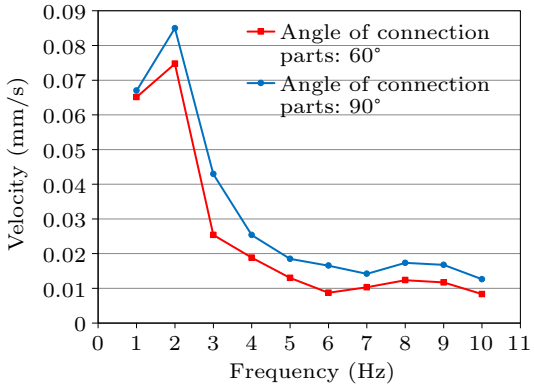


Fig. 26. Number of walks at each frequency.

4.3. Moving work rate

To evaluate the energy efficiency of a propulsive motion, the moving work rate (cost of transport (COT)) was calculated. The moving work rate is the dimensionless amount of energy required by moving the unit mass unit distance, expressed by formula (4) of power consumption P [in units of J/s], velocity U [in units of m/s], and mass M [in units of kg].

$$\mathrm{COT} = \frac{P}{M \cdot U}, \tag{4}$$

COT = 70.3 and 67.7 when the maximum swimming speed is 2 Hz and the angles of the connector are 90° and 60°, respectively.

5. Conclusions

To improve the performance of robot fish, this project developed a robot fish with a DEA that can imitate the bending motion of the fish body and tail fin.

First, to incorporate the motion of a planar stretch-shrinkable DEA into the bending motion, a DEMES was used to make a bending driver. The resulting drive produced an angle change of 42.2° at 4 kV. The result is a higher response

frequency of 5.9 Hz than that of the flat driver, which can be used to mimic the swimming motion of fish.

Second, with respect to the curved movement of the fish's body and tail fin, a robotic fish was also developed that aims to mimic the swimming patterns of subcarangiform and carniform fish. A drive unit capable of bending left and right using a bending drive was made. The drive unit uses a structure that directly glues one end of two bent drives and connects the other end by connecting pieces. The connecting pieces obtain a maximum force at 60° and a maximum angle change at 90°. When driving the drives on both sides at 4 kV, the connector angle changes the maximum angle at 60° to 18.7, and the connector angle changes the maximum angle at 90° to 21.1. When the connector angle is 60°, the response frequency of the driver is 6.1 Hz; at the 90° connector angle, the drive responds at 6.4 Hz, so it can be used to mimic fish swimming.

The tail fin was connected to the driving unit, the robot fish was made, and the swimming experiment was carried out. The swimming experiment results revealed that when the frequency was 2 Hz, the angle of the connector was 60°, the swimming speed was 14.2 mm/s, the angle of the connector was 90°, and the swimming speed was 16.1 mm/s.

Acknowledgements

Project supported by Joint Open Fund of Guizhou Provincial Department of Education (Grant No. [2022] 439) and the Academic New Seedling Cultivation and Free Exploration and Innovation of Guizhou Provincial Science and Technology Department (Grant No. [2023] 11).

References

[1] Chidsey C E D and Murray R W 1986 *Science* **231** 4733
[2] Wissler M and Mazza E 2007 *Sensors and Actuators A: Physical* **138** 384
[3] Keplinger C, Kaltenbrunner M, Arnold N and Bauer S 2010 *Proc. Natl. Acad. Sci. USA* **107** 4505
[4] Dong L, Liu B, Wang Y and Xu X 2022 *Chin. Phys. Lett.* **39** 127201
[5] Kornbluh R D, Pelrine R, Joseph J, Heydt R, Pei Q and Chiba S 1999 *Smart Structures and Materials* **3669**
[6] Rus D and Tolley M T 2015 *Nature* **521** 7553
[7] Brochu P and Pei Q 2010 *Macromolecular Rapid Communications* **31** 10
[8] Tavakol B and Holmes D P 2016 *Appl. Phys. Lett.* **108** 112901
[9] He B, Zhang C H and Ding A 2017 *Chin. Phys. B* **26** 126102
[10] Ren Z, Kim S, Ji X, Zhu W, Niroui F, Kong J and Chen Y 2022 *Adv. Mater.* **34** 2106757
[11] Chen J, Zhou X and Zhang L 2018 *Chin. Phys. B* **27** 118701
[12] Tang C, Du B, Jiang S, Shao, Q, Dong X, Liu X J and Zhao H 2022 *Science Robotics* **7** 66
[13] Liu Y, Chen B, Li W, Zu L, Tang W and Wang Z L 2021 *Adv. Funct. Mater.* **31** 2104770
[14] Godaba H, Li J, Wang Y and Zhu J 2016 *IEEE Robotics and Automation Letters* **1** 2
[15] Jiao Z W, Wang H Y, Luo B, Yang W M and Yu Y 2022 *J. Phys.: Conf. Series* **2331** 012010
[16] Shintake J, Shea H and Floreano D 2016 *IEEE/RSJ International Conference on Intelligent Robots and Systems* (*IROS*)
[17] Tang Y, Qin L, Li X, Chew C M and Zhu J 2017 *IEEE/RSJ international conference on Intelligent Robots and Systems* (*IROS*)
[18] Wang S, Huang B, McCoul D, Li M, Mu L and Zhao J 2019 *Smart Materials and Structures* **28** 045006
[19] Xu J, Dong Y, Yang J, Jiang Z, Tang L, Chen X and Cao K 2023 *Soft Robotics* **10** 2
[20] Zhang C W, Zou W, Yu H C, Hao X P, Li G, Li T and Zheng Q 2022 *ACS Appl. Mater. Interfaces* **14** 52430
[21] Wang G Q, Luo H and Hu X X 2018 *Chin. Phys. B* **27** 028901